Structure of Botulinum Neurotoxin Type D Light Chain at 1.65 Å Resolution: Repercussions for VAMP-2 Substrate Specificity[†,‡]

Joseph W. Arndt,[§,||] Qing Chai,[§,||] Todd Christian,[⊥] and Raymond C. Stevens*[,§]

Department of Molecular Biology, The Scripps Research Institute, 10550 North Torrey Pines Road, La Jolla, California 92037, and List Biological Laboratories, Inc., 540 Division Street, Campbell, California 95008

Received December 9, 2005; Revised Manuscript Received January 17, 2006

ABSTRACT: The seven serotypes (A−G) of botulinum neurotoxins (BoNTs) function through their proteolytic cleavage of one of three proteins (SNAP-25, Syntaxin, and VAMP) that form the SNARE complex required for synaptic vesicle fusion. The different BoNTs have very specific protease recognition requirements, between 15 and 50 amino acids in length depending on the serotype. However, the structural details involved in substrate recognition remain largely unknown. Here is reported the 1.65 Å resolution crystal structure of the catalytic domain of BoNT serotype D (BoNT/D-LC), providing insight into the protein−protein binding interaction and final proteolysis of VAMP-2. Structural analysis has identified a hydrophobic pocket potentially involved in substrate recognition of the P1′ VAMP residue (Leu 60) and a second remote site for recognition of the V1 SNARE motif that is critical for activity. A structural comparison of BoNT/D-LC with BoNT/F-LC that also recognizes VAMP-2 one residue away from the BoNT/D-LC site provides additional molecular details about the unique serotype specific activities. In particular, BoNT/D prefers a hydrophobic interaction for the V1 motif of VAMP-2, while BoNT/F adopts a more hydrophilic strategy for recognition of the same V1 motif.

Botulinum neurotoxins (BoNTs)[1] are the most potent toxins known in nature, causing long-lasting paralysis and death through the inhibition of neurotransmitter release from cholinergic synapses. Botulism is caused by the anaerobic bacteria of the genus *Clostridium*. There are seven serotypes of clostridial BoNTs (serotypes A−G), which were designated in chronological order of their discovery. BoNT types A, B, E, and F are implicated in human cases, while types C and D appear to cause only animal botulism. BoNT/D was first isolated from an outbreak of botulism in cattle in South Africa (*1*). However, recently, sporadic cases have also been documented in Africa, Europe, and North and South America (*2*, *3*); thus, it is of global concern. Notably, BoNT/D is harmless to humans because of the lack of a specific receptor on human neurons (*4*). Therefore, BoNT/D has also been utilized as a molecular instrument in neurobiology for delivery of various biomolecules (*5*).

Clostridial BoNTs are produced as 150 kDa single-chain proteins that are subsequently cleaved by either intrinsic or host proteases to yield a disulfide-linked di-chain composed of an ∼100 kDa heavy chain (HC), encompassing the cell binding and translocation units, and an ∼50 kDa enzymatic light chain (LC) (*6*). BoNT-LCs belong to the superfamily of zinc endoproteases that possess a His-Glu-X-X-His motif (HExxH) at the active site for metal coordination (*7*). Their substrates have been found to be one of three proteins that interact to form a multimeric ensemble named the SNARE (soluble *N*-ethylmaleimide-sensitive factor attachment protein receptor) complex, which is required for vesicle fusion and transmitter release. BoNT/A and BoNT/E proteolyze SNAP-25 (synaptosomal-associated 25 kDa protein); BoNT/B, /D, /F, and /G cleave VAMP (vesicle-associated membrane protein), also known as synaptobrevin, and BoNT/C cleaves syntaxin as well as SNAP-25 (*7*). BoNT-induced cleavage of their SNARE substrates greatly diminishes the efficacy of the complex; as a result, the BoNTs have become important therapeutic agents for the treatment of neurological disorders, as well as vital biological tools for probing exocytosis events.

All BoNT-LCs bear a similar three-dimensional structure, yet they show remarkable differences in substrate specificity. They are in fact the most selective proteases that have been identified (*8*). A wealth of biochemical evidence has shown the BoNTs do not tolerate amino acid substitutions adjacent to the scissile bond on the C-terminal side (P1′ position) (*9*−*11*). Combining sequence and structural analysis indicates that the specificity of BoNT-LCs is mainly due to a spatial

[†] This work was supported by Pacific Southwest Regional Center of Excellence Grant U54 AI065359. Portions of this research were carried out at the Advanced Light Source, which is supported by the Director, Office of Science, Office of Basic Energy Sciences, of the U.S. Department of Energy under Contract DE-AC02-05CH11231.

[‡] The coordinates for the structure have been deposited in the Protein Data Bank as entry 2FPQ.

* To whom correspondence should be addressed. Phone: (858) 784-9416. Fax: (858) 784-9483. E-mail: stevens@scripps.edu.

[§] The Scripps Research Institute.

[||] These authors contributed equally to this work.

[⊥] List Biological Laboratories, Inc.

[1] Abbreviations: BoNT, botulinum neurotoxin; CV, column volumes; DTT, dithiothreitol; GST, glutathione *S*-transferase; HC, heavy chain; LC, light chain; PBS, phosphate-buffered saline; SNAP-25, synaptosomal-associated 25 kDa protein; SNARE, soluble *N*-ethylmaleimide-sensitive factor attachment protein receptor; SSR, SNARE secondary recognition; TeNT, tetanus neurotoxin; TSA, transition-state analogue; V1, first SNARE motif in VAMP; V2, second SNARE motif in VAMP; VAMP, vesicle-associated membrane protein.

10.1021/bi052518r CCC: $33.50
Published on Web 02/14/2006

and conformational organization of the active site and exosite recognition regions. Contributing to the exosites are the sequence conservation regions that consist of nine-residue conserved regions, known as the SNARE motifs. They are found in all SNARE substrates, though not all of them are necessary for recognition and interaction. For instance, in VAMP-2 there are two copies of this motif, termed V1 and V2, with only V1 being important in substrate discrimination by BoNT/D (*12*). Although it is clear that progress is being made in defining the interaction between the toxin and substrate, there is still much to be learned. Here we report the expression, purification, and crystal structure determination of BoNT/D-LC to 1.65 Å resolution.

EXPERIMENTAL PROCEDURES

Expression and Purification of BoNT/D-LC. Overexpression of BoNT/D-LC (residues 1−436) was induced with isopropyl α-thiogalactopyranoside under control of the *tac* promoter in plasmid pGEX-6P-1 (Amersham Biosciences). This plasmid encodes an expression and purification tag consisting of the glutathione *S*-transferase (GST) gene from *Schistosoma japonicum* fused at the N-terminus of the LC protein. Bacteria were lysed by sonication in phosphate-buffered saline (PBS) supplemented with EDTA-free protease inhibitor tablets (Roche) and 0.1 mg/mL lysozyme. Immediately after sonication, the cell debris was pelleted by centrifugation. The soluble fraction was mixed with glutathione−Sepharose 4B resin (Amersham Biosciences) equilibrated in PBS at 4 °C for 2 h and then poured into a gravity flow column. The resin was drained and washed with 5 column volumes (CV) of PBS and with 2 CV of cleavage buffer [50 mM Tris (pH 7.0), 150 mM NaCl, and 1 mM DTT]. The GST tag was cleaved from the LC protein with PreScission protease (Amersham Biosciences) overnight at 4 °C. BoNT/D-LC was eluted and washed from the resin with cleavage buffer. The purified protein was exchanged with 20 mM Tris (pH 8.0) and 50 mM NaCl by centrifugal ultrafiltration using an Amicon Ultra-15 centrifugal filter device with a molecular mass cutoff of 10 kDa. The protein was then concentrated to 11 mg/mL (Orbital) and either frozen in liquid nitrogen for later use or used immediately for crystallization trials.

Activity Assay. An endopeptidase assay was used to assess the activity of the purified BoNT/D-LC. BoNT/D-LC (20 nM) and VAMP-2 (5 μM) were incubated in 100 μL of reaction buffer [20 mM Tris (pH 8.0) and 50 mM NaCl] at 37 °C. Sample aliquots (20 μL) were removed at various time points and the reactions quenched with SDS gel-loading buffer. The samples were run and visualized on an 18% polyacrylamide gel. The digestion of VAMP-2 could be seen within 5 min of initiation of the endopeptidase reaction.

Crystallization and Cryoprotection of BoNT/D-LC. The protein was crystallized by the nanodroplet vapor diffusion method (*13*) using the Innovadyne Screenmaker crystallization robot (drop-size: 200 nL) and kept at 277 K. Plate-shaped crystals of diffraction quality grew in 1−3 days in a crystallization solution that contained 15% PEG 4000, 200 mM potassium thiocyanate, and 100 mM sodium acetate at pH 5.5. Crystals (0.2 mm × 0.2 mm × 0.02 mm) were transferred to mother liquor solutions of increasing concentrations of PEG 550 MME (up to 15%) prior to being harvested with LithoLoops (Molecular Dimensions Ltd.) and flash-frozen in liquid nitrogen.

Table 1: Summary of Data Collection and Refinement Statistics for BoNT/D-LC (PDB entry 2FPQ)

Data Collection	
space group	$P2_1$
unit cell parameters	$a = 146.8$ Å, $b = 89.8$ Å, $c = 54.4$ Å, $\beta = 94.3°$
resolution range (Å)	50.00−1.65
highest-resolution shell (Å)	1.71−1.65
no. of observations	663503
no. of reflections	48292
completeness (%)	95.2 (93.3)[a]
mean I/σ (I)	21.6 (2.2)[a]
R_{sym}[b] on I	0.049 (0.546)[a]
Model and Refinement Statistics	
resolution range (Å)	44.9−1.65
no. of reflections (total)	48292
no. of reflections (test)	2594
completeness (% of total)	94.9
R_{cryst},[c] R_{free}[d]	0.182, 0.219
Stereochemical Parameters	
restraints (rmsd observed)	
bond lengths (Å)	0.019
bond angles (deg)	1.715
no. of protein residues, no. of atoms	414, 3404
no. of solvent molecules	375
no. of heterogeneous atoms	2

[a] Highest-resolution shell. [b] $R_{sym} = \sum|I_i - \langle I_i\rangle|/\sum|I_i|$, where I_i is the scaled intensity of the ith measurement and $\langle I_i\rangle$ is the mean intensity for that reflection. [c] $R_{cryst} = \sum||F_{obs}| - |F_{calc}||/\sum|F_{obs}|$, where F_{calc} and F_{obs} are the calculated and observed structure factor amplitudes, respectively. [d] R_{free}, as for R_{cryst}, but for 5.0% of the total reflections chosen at random and omitted from the refinement.

Data Collection. Diffraction data were collected at the Advanced Light Source (ALS) on beamline 8.2.1 at a wavelength of 1.000 Å. The data set was collected at 100 K using an ADSC q210 CCD detector. Data were integrated, reduced, and scaled using HKL2000 (*14*). The crystal was indexed in monoclinic space group $P2_1$, as predicted from the observed systematic absences; data statistics are summarized in Table 1.

Structure Determination and Refinement. The structure was determined by molecular replacement using the BoNT/G-LC structure [PDB entry 1ZB7 (*15*) with 39% sequence identity] as the search model with MolRep (*16*). The model was manually built with Coot (*17*). Structure refinement was performed using REFMAC5 (*18*). The progress of the model refinement was monitored by a cross-validation R_{free} (*19*), which was computed from a randomly assigned test set comprising 5% of the data. Refinement statistics are summarized in Table 1. The final model includes a single protein molecule and 375 water molecules. No electron density was observed for residues 206−214, 175−177, and 425−436. Analysis of the stereochemical quality of the model was accomplished using AutoDepInputTool (http://deposit.pdb.org/adit/). Figures were prepared with PYMOL (DeLano Scientific). Atomic coordinates and experimental structure factors of BoNT/D-LC have been deposited with the Protein Data Bank as entry 2FPQ.

Substrate Modeling. The substrate-bound crystal structure of BoNT/A1 bound to SNAP-25 (PDB entry 1XTG) (*20*) was used to model BoNT/D-LC with its VAMP-2 substrate, by superpositioning the structures with TOP (*21*). The BoNT/A1-SNAP-25 orientation that was used introduces comple-

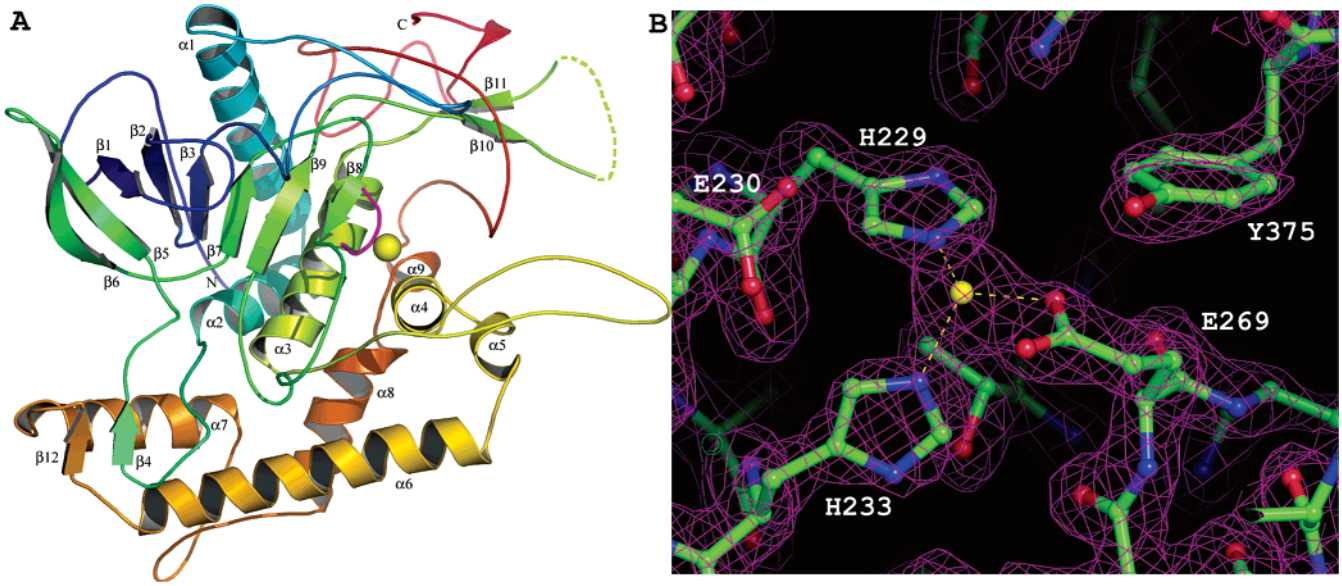

FIGURE 1: Crystal structure of BoNT/D-LC. (A) Ribbon diagram of *C. botulinum* BoNT/D-LC rainbow colored with the N-terminus in blue and the C-terminus in red. β-Strands ($\beta1-\beta12$) and α-helices ($\alpha1-\alpha9$) are labeled. The active site zinc ion is shown as a yellow sphere. The second conformation of the active site $\beta8$ strand is colored magenta. The dashed line corresponds to residues 206−214, which are not modeled in the structure. (B) Active site HExxH motif superimposed on the $2F_o - F_c$ electron density map contoured at 1σ. The fourth ligand is a water molecule that is not shown for clarity.

mentary interactions between VAMP-2 and BoNT/D-LC that are in agreement with biochemical and mutational studies (*12*, *22*). The details of the interactions near the cleavage site, in particular the S1′ subsite, were elucidated by a similar comparison of BoNT/D-LC with the structure metalloprotease thermolysin bound to a transition-state analogue (PDB entry 4TMN) (*23*).

RESULTS AND DISCUSSION

Structure of BoNT/D-LC

The final model of the BoNT/D-LC structure (Figure 1A) is composed of twelve β-strands ($\beta1-\beta12$), nine α-helices ($\alpha1-\alpha9$), and two 3_{10}-helical segments ($\eta1$ and $\eta2$). The active site has the geometry and coordination typical of the zinc-binding HExxH motif found in the other BoNTs. The active site zinc is coordinated by His 229 and His 233 of the HExxH motif (Figure 1B). Completing the tetrahedral zinc coordination are Glu 269 and a water molecule.

Intriguingly, two conformations of the active site β-strand ($\beta8$) are observed in the BoNT/D-LC structure (Figure 1A). The first is typical of BoNT-LCs in that it packs against the active site β-sheet in an antiparallel fashion to form an eight-stranded β-sheet with 65123798 topology. This is likely to be the physiologically relevant conformation, with regard to VAMP substrate recognition, since all BoNT-LCs have this structural signature. The second conformation is a random coil occupying roughly the same position occupied by the belt region. This alternate conformation may be due to the low occupancy of the active site zinc ion (70%) or could be an early unfolding transition into a molten globule state required for the pH-dependent LC translocation (*24*, *25*).

The overall structure of BoNT/D-LC is similar to the other serotypes of BoNT/A (*20*, *26*), /B (*27*), /E (*28*), /F (*29*), and /G (*15*) and the tetanus neurotoxin LC (TeNT) (*30*, *31*) (Figure 2A). Their structural similarity is evident in DALI *Z*-scores (*32*) obtained by superposing the C_α atoms of BoNT/D-LC and the other known BoNT-LCs (A, 46.1; B, 47.3; E, 47.2; F, 47.2; and G, 45.7). The closest structural homologue of BoNT/D-LC is the TeNT-LC (*30*) with a DALI *Z*-score of 49.6. BoNT/D-LC can be superposed on TeNT-LC with a C_α rmsd of 2.3 Å for the 382 structurally equivalent residues used in the superposition. This structural likeness among the BoNT-LCs and TeNT-LC is based on the thermolysin-like α/β core shared by all of the LCs that contributes approximately 25% of the total structure of the BoNTs and comprises most of the secondary structure features (Figure 2B). It is likely the clostridial neurotoxins have developed from an ancestral thermolysin-like hydrolase for their proteolytic scaffold and diverged for their specific targets of the SNARE exocytosis fusion machinery (Figure S1 of the Supporting Information) (*33*). The major structural differences are observed mainly in loop regions and their C-termini, particularly with loops 30, 50, 140, 180, 200, 250, 315, and 340 (Figure 2A,B). The BoNT/D-LC structure is one of the few LC structures in which the 250 loop has been observed. This loop has been known to undergo conformational change upon substrate binding (*27*, *20*). It is visible in the BoNT/D-LC structure due to Phe 257 and Phe 258 at the end of the 250 loop packing into a hydrophobic pocket in a symmetry-related molecule. On the basis of the structural diversity observed in the 250 loop and other loops in the LC crystal structures, these regions are expected to be highly flexible under physiological conditions and likely contribute to substrate specificity, though crystal packing at these loop regions may also contribute to the structural plasticity observed in the BoNT-LC structures. Our analysis shows that there is a correlation between structural plasticity observed in these loops among the different serotypes with respect to their amino acid sequence variability (Figure S2 of the Supporting Information). This is evident by the loop regions having a low degree of sequence identity (~3%). Phenotypic and genotypic studies have demonstrated the

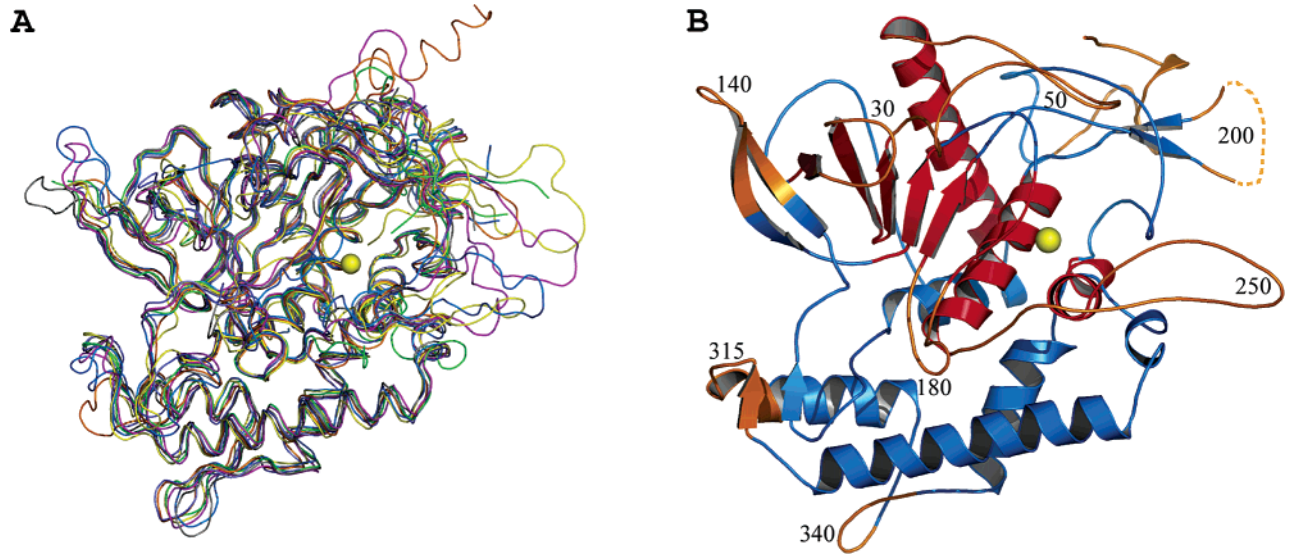

FIGURE 2: Overall BoNT/D-LC structure compared to other BoNT- and TeNT-LCs. (A) A coil representation of a C_α superposition of LC structures from BoNT/A (yellow), BoNT/B (magenta), BoNT/D (marine blue), BoNT/E (orange), BoNT/F (slate), and TeNT (black) showing their structural similarity. (B) Ribbon diagram of BoNT/D-LC colored blue with the thermolysin-like core in red and structurally variable regions in orange with loops indicated. The active site zinc ion is shown as a yellow sphere.

presence of four distinct lineages among *Clostridium botulinum* producing neurotoxins. Serotypes A, B, and F belong to group I, and serotype E belongs to group II; the closely related C and D serotypes belong to group III, and serotype G belongs to group IV (*34*). This is slightly different from our analysis of the amino acid sequences of all neurotoxin LCs that shows that serotypes B and G are more closely related (Figure S1 of the Supporting Information). Since nucleotide sequence comparison of BoNT genes does not agree with the four phylogenetic groups of organisms, it is been suggested that lateral gene transfer, such as transposons, plasmids, and bacteriophages, accounts for spreading of the gene element between serotypes (*35*). However, there is no apparent phylogenetic evidence pointing out the relationship among either the VAMP specific BoNTs or SNAP-25 specific BoNTs. Despite the wealth of genetic, biochemical, and structural information available for the neurotoxins, it is clear that there is a long way to go before they are thoroughly understood.

Putative VAMP Recognition Sites for BoNT/D-LC

S1′ Subsite of BoNT/D-LC. The site of BoNT/D-LC cleavage in VAMP-2 is between the two SNARE motifs, V1 and V2, at the Lys 59-Leu 60 bond. To assess the details involved in the recognition of VAMP-2 by BoNT/D, its structural comparison was performed against the LC crystal structure of BoNT/A in complex with its SNARE substrate. Our structural analysis suggests that BoNT/D-LC shares a similar orientation of substrate binding observed in the BoNT/A-LC−SNAP-25 complex with the substrate in an extended β-strand conformation running antiparallel to active site β-strand β8. To our knowledge, this is the preferred orientation of substrate binding for HExxH-containing proteases.

The antiparallel orientation clearly complements the P1′ Leu 60 residue of VAMP-2 with respect to its putative S1′ subsite of BoNT/D-LC. BoNTs have a strict dependence for the P1′ residues of their SNARE substrates (*9*−*11*, *36*). The P1′ residues are chemically dissimilar, varying in both size and chemical nature. Therefore, it is expected that each BoNT serotype would have a complementary S1′ subsite for recognition of this structurally varied pool of P1′ residues of their SNARE substrates. The S1′ subsite has been identified for BoNT/E (*37*), BoNT/F (*29*), and BoNT/G (*15*). Here we show that a similar approach of modeling with BoNT/D-LC with the structurally equivalent region of thermolysin (*23*) suggests the S1′ subsite of BoNT/D. The P1′ leucine residue of the VAMP is directed toward a shallow hydrophobic pocket forming the S1′ subsite of BoNT/D-LC that is composed of Tyr 168, Leu 200, Met 221, and Ala 226 (Figure 3). This is different than the S1′ subsite proposed for BoNT/D that is based on homology modeling with the BoNT/F-LC structure (*37*), which speculates that the P1′ recognition occurs through Tyr 168, Leu 199, and Ala 226.

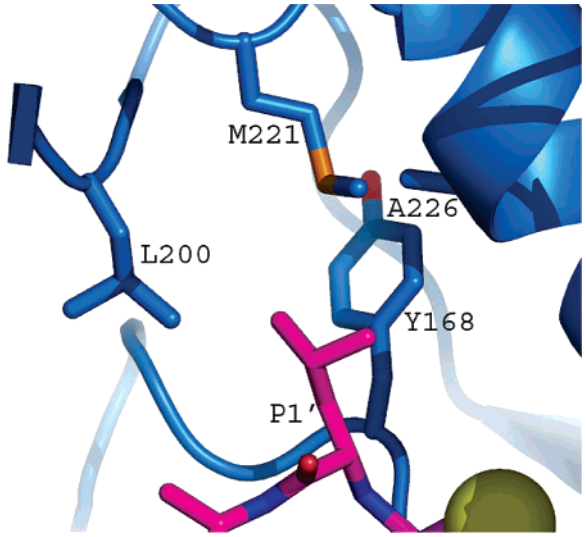

FIGURE 3: Close-up view of the putative S1′ subsite of BoNT/D-LC at the P1′ region. S1′-binding residues as observed in BoNT/D-LC (blue) modeled with P1′ leucine (magenta) with oxygens (red), nitrogens (blue), and sulfur (orange). The P1′ residue of the substrate (Leu 60 of VAMP-2) is surrounded by Tyr 168, Leu 200, Met 221, and Ala 226 of BoNT/D-LC. The active site zinc ion is shown as a yellow sphere.

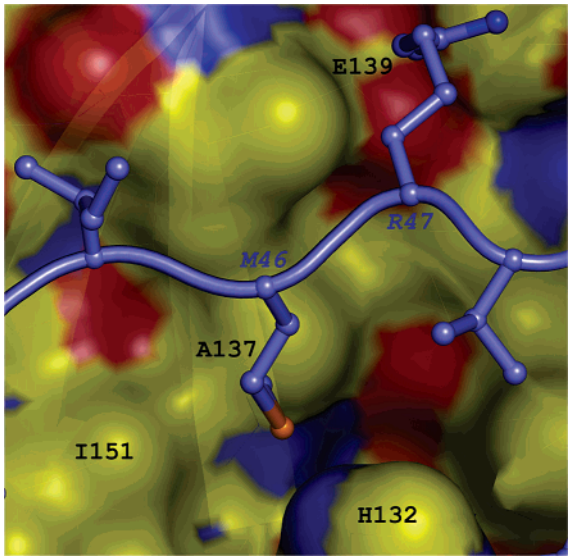

FIGURE 4: Close-up view of the putative V1 exosite of BoNT/D-LC. A semi-transparent surface representation of the putative V1 binding site as observed in BoNT/D-LC with carbons (yellow), nitrogens (blue), oxygens (red), sulfurs (orange), and the modeled VAMP-2 (slate blue). V1 residues Met 46 and Arg 47 of VAMP-2 (labeled blue italics) are surrounded by His 132, Ala 137, Glu 139, and Ile 151 of BoNT/D-LC.

This sequence-based prediction fails because Leu 199 is buried in the hydrophobic core of the protein; therefore, it could not participate in P1′ discrimination. In addition, the BoNT/D-LC structure shows that Leu 200 and Met 221, two residues missing in the homology model, line this pocket and are likely to be involved in hydrophobic interactions with the P1′ Leu of VAMP-2.

Recognition of the SNARE Motifs of VAMP. Outside of the active site region, the cleavage of VAMP-2 has been shown to be susceptible to mutation of residues in the V1 SNARE secondary recognition (SSR) motif (residues 39−47), with a key residue being Met 46 (*12*). In agreement with these findings, Yamasaki and colleagues showed that VAMP-1 required an almost 3700-fold higher concentration of BoNT/D to achieve the same cleavage observed with VAMP-2 in vitro (*22*). The drastic difference in the two VAMP isoforms was attributed to a Met 46 to Ile substitution in VAMP-1. In our docked model, this critical Met 46 of VAMP-2 is buried in a pocket of BoNT/D-LC composed of His 132, Ala 137, and Ile 151 (Figure 4). The side chain of Met 46 fits into the hydrophobic pocket with its sulfur making a potential hydrogen bond with the imidazole nitrogen of His 132 of BoNT/D. This model helps to clarify the troubling question of why recombinant rat VAMP-1 is such a poor substrate for BoNT/D as compared to the VAMP-2 isoform. Though this is a conservative substitution in terms of hydrophobic nature, the lack of a hydrogen-bonding acceptor as found in the Met 46 sulfur likely contributes to the difference in the affinities of the VAMP isoforms. Possibly, Met 46, together with Val 42, Val 43, and Ile 45 of VAMP-2, forms a hydrophobic patch for contacts with BoNT/D-LC. Additionally, a salt bridge between Glu 139 of BoNT/D-LC and Arg 47 of VAMP-2 is also likely.

On the basis of the observed cleavage rates of N- and C-terminal truncations of rat VAMP-2 (22), the minimum length of substrate of BoNT/D is likely to be from Thr 27 to Gln 76. Shorter peptides with 15 residues on either side of the scissile bond (Lys 59-Leu 60) were not cleaved at all, indicating that the V2 SSR (residues 63−71) is also important in recognition by BoNT/D. Similar substrate length constraints are also required for BoNT/A activity (*38*). Nonetheless, mutational analysis of residues in the V2 motif failed to identify amino acids that are critical for BoNT/D activity. On the other hand, complementary side chain interactions are not necessarily anticipated, since this equivalent region on SNAP-25 in the BoNT/A−substrate complex, termed the β-exosite, forms a short β-sheet with the 250 loop through main chain hydrogen-bonding interactions (Figure 5). Assuming a similar mode of binding, the V2 SSR of VAMP-2 would form a short β-sheet between Asp 261 and Gly 262

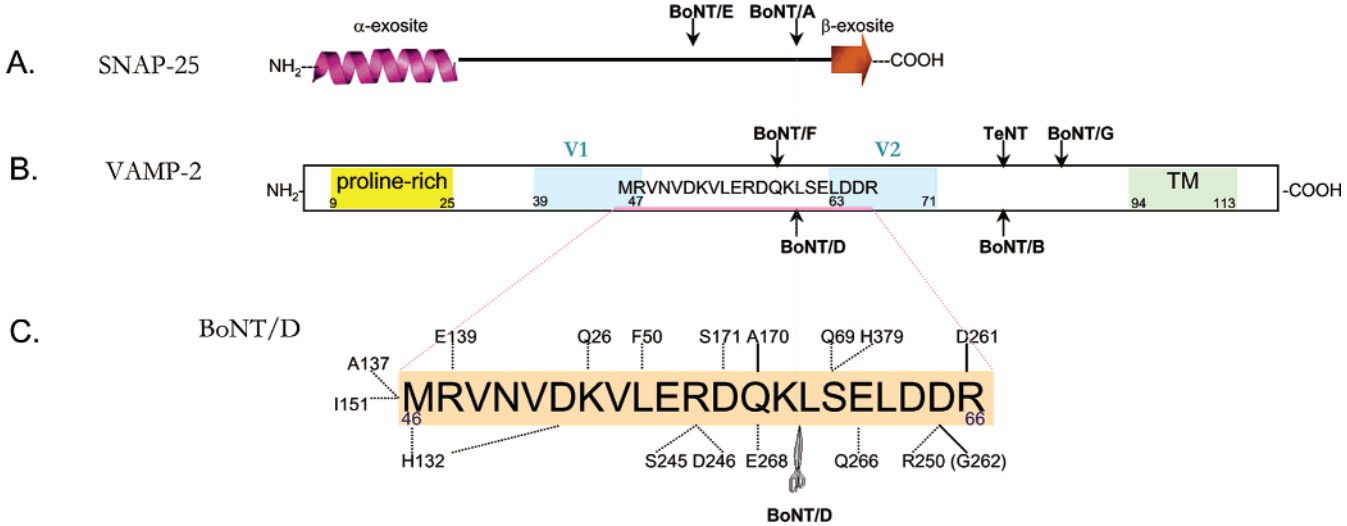

FIGURE 5: Comparison of BoNT substrate specificity. (A) SNAP-25 is shown schematically as an N-terminal α-helix followed by a random coil and a short β-strand at the C-terminus. Arrows indicate the cleavage sites of BoNT/A and /E. (B) Schematic structure of rat VAMP-2. The N-terminal proline-rich region is highlighted in yellow; the V1 and V2 motifs are colored blue, and the C-terminal transmembrane domain (TM) is colored green. Arrows indicate the cleavage sites of BoNT/D, /F, /B, and /G and TeNT. (C) Modeled interactions between the BoNT/D-LC structure and the VAMP-2 substrate. Residues of VAMP-2 underlined in panel B are shown in an orange-shaded box (Met 46−Arg 66). Putative substrate binding residues of BoNT/D are indicated. They form either side chain (dotted line) or main chain (solid line) interactions with specific residues of VAMP-2.

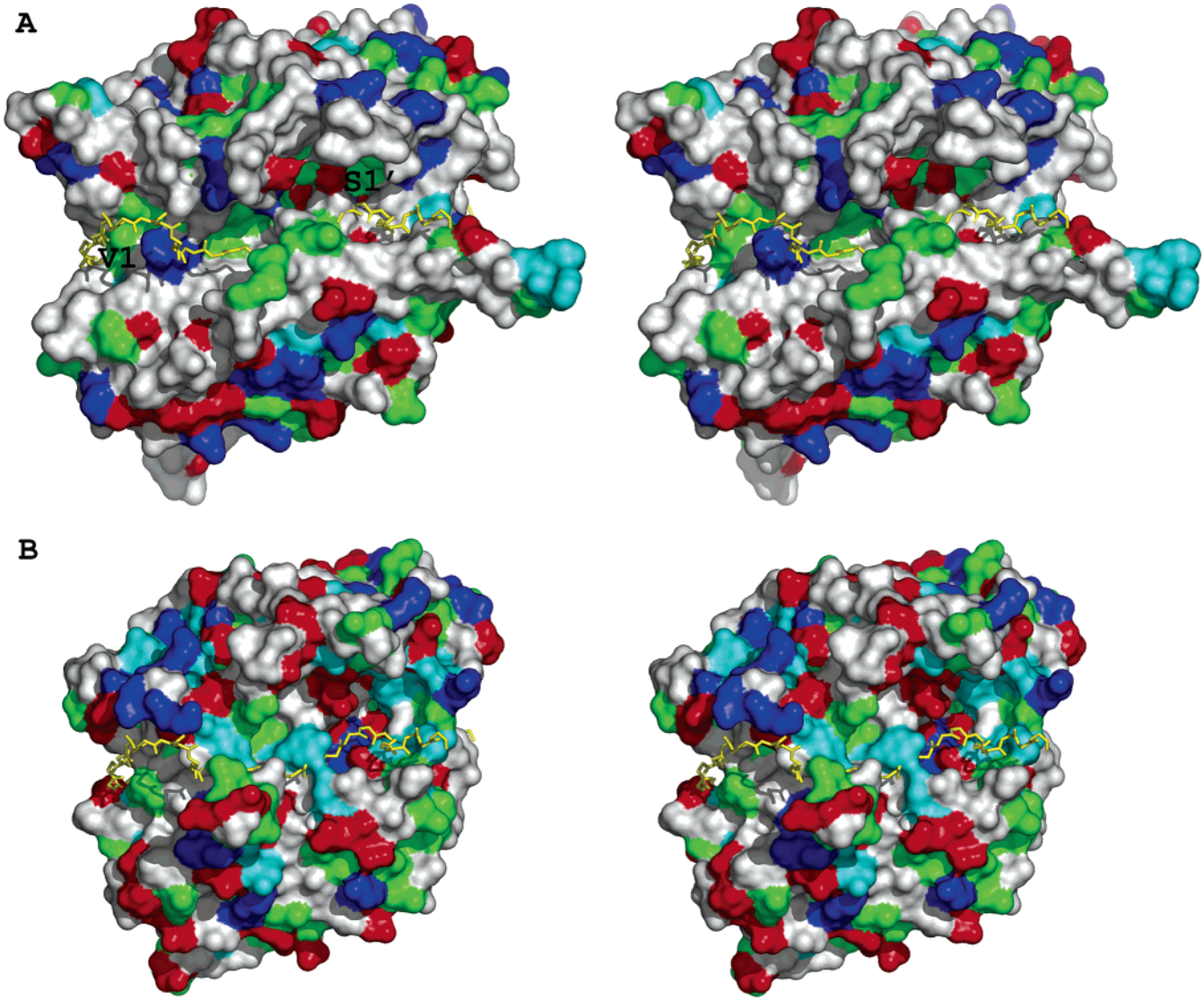

FIGURE 6: Stereoview of modeled substrate binding channel differences between BoNT/D-LC and BoNT/F-LC. (A) BoNT/D-LC and (B) BoNT/F-LC are colored according to surface residue type with aromatic (cyan), hydrophobic (green), acidic (red), and basic residues (blue) superposed on the putative model of the main chain residues of the VAMP-2 substrate (yellow).

of the 250 loop of BoNT/D-LC with Asp 65 and Arg 66 of VAMP-2. Contributing to the BoNT/D β-exosite, an additional salt bridge between Arg 250 of BoNT/D-LC and Asp 65 of VAMP-2 is also anticipated.

Unique Characteristics in the Recognition of VAMP by BoNT/D-LC. Though our model appears to be similar to the orientation of the substrate observed in the BoNT/A-LC−SNAP-25 complex, there is a noteworthy difference. In the BoNT/A-LC−SNAP-25 structure, an extensive interface, termed the α-exosite, is observed on the posterior side of BoNT/A with an α-helix at the N-terminus of SNAP-25. The equivalent region in VAMP-2 is a proline-rich motif (residues 9−25) containing nine prolines (Figure 5). This motif precludes the likelihood of a helical interaction for BoNT/D and /F at the α-exosite seen in the BoNT/A-LC−SNAP-25 complex. This is due to the fact that prolines are well-known to be helix breakers, so many in such a small stretch would certainly not be expected to form a helix. Therefore, the speculation that all serotypes have a similar mode of binding to SNAP-25 (*39*) observed in the BoNT/A-LC−SNAP-25 complex is not likely to hold for BoNT/D and /F. However, the proline-rich motif does not rule out the existence of an α-exosite for the other VAMP specific neurotoxins, BoNT/B and /G and TeNT, since they all have a downstream cut site relative to BoNT/D and /F (Figure 5). In fact, removal of this proline-rich domain does not compromise substrate binding for BoNT/D and /F (*22*). Nonetheless, this proline-rich region is still clearly important in exocytosis, because its deletion inhibits the process, and peptides resembling this N-terminal region inhibit neurotransmitter release (*40*). It has also been noted that N-terminus of VAMP does not contribute to the structure of the four-helix bundle of the SNARE complex but instead makes up a cytoplasmic extension (*7*). Since the minimum substrate length is the Thr 27−Gln 76 segment, C-terminal interactions of VAMP-2 on the backside of BoNT/D-LC are possible.

Additional interactions contributing to substrate binding in our model at the C-terminal side of the scissile bond include hydrogen bonds between P2′ Ser 61 and Gln 69 and His 379 of BoNT/D, as well as between Glu 62 of VAMP and Gln 266 of BoNT/D (Figure 5). On the N-terminal cleavage side, hydrophobic packing, such as Leu 54 of VAMP with Phe 50 of BoNT/D, and more hydrogen-bonding, involving the P2−P4 residues of VAMP, are

anticipated. From this model provided by the BoNT/A-LC−SNAP-25 complex (*20*), it seems that binding of substrate is extensive. These interactions described above with those involved in the binding of the V1 SSR and the β-exosite give an explanation for the length-dependent effects of BoNT/D-LC. In the case of BoNT/D-LC, V1 recognition of the critical Met 46 and Arg 47 of VAMP-2 may act as an anchor point for the proper orientation and guidance of the substrate. Then V2 SSR recognition by the 250 loop of BoNT/D likely increases the affinity by forming a short β-sheet. Finally, recognition at the active site is expected with Leu 60 of VAMP being drawn into the S1′ pocket preparing for cleavage. It is clear that exosites are critical for molecular recognition that governs BoNT-LC function. Nonetheless, further kinetic study of various mutants and complex structures with VAMP-2 are required to elucidate the sequential and directional model of substrate recognition.

In contrast to BoNT/F-LC, the BoNT/D-LC structure shows a surface residue distribution in the substrate binding channel that is more hydrophobic, while BoNT/F-LC is more charged (Figure 6). This difference in the chemical nature in the substrate-binding channels between the two VAMP specific serotypes is consistent with in vitro activities and the observed mutational analysis of the two neurotoxins. BoNT/D-LC can efficiently cleave VAMP-2 in the presence of a high concentration of salt since this would strengthen the hydrophobic interaction between the enzyme and substrate. However, BoNT/F that cleaves the adjacent peptide bond (Gln 58-Lys 59) on VAMP does not have activity under similar assay conditions (*12*). In this case, the highly ionic environment likely disrupts the electrostatic interface between BoNT/F and VAMP. Furthermore, this structural analysis also adds some chemical perspective to the biochemical evidence that BoNT/D activity is vulnerable to mutation of the hydrophobic Met 46 of VAMP, while BoNT/F is more susceptible to Asp 40, Glu 41, and Asp 44 mutations (*12*). Taken together, it is likely that hydrophobic contacts provide the major binding energy for interaction of the V1 motif with BoNT/D.

Structural mapping of all the BoNT-LCs is almost complete, with the exception of serotype C that has yet to be determined. This enrichment of molecular diversity of BoNT-LCs has shed some light on the details responsible for substrate recognition. The structure of BoNT/D-LC presented here provides a chemical foundation for the specificity for the P1′ residue and the V1 SNARE motif of VAMP-2. However, additional work is required on fully functional BoNT−substrate co-crystal structures that to date have remained a formidable challenge, even with significant efforts to obtain such structural information (*15*, *20*, *26*−*31*).

ACKNOWLEDGMENT

We thank Angela Walker for assistance with manuscript preparation and Fay Bi for technical support.

SUPPORTING INFORMATION AVAILABLE

Phylogram of BoNT-LCs with TeNT and thermolysin (Figure S1) and sequence alignment of BoNT-LCs (Figure S2). This material is available free of charge via the Internet at http://pubs.acs.org.

REFERENCES

1. Meyer, K. F., and Gunnison, J. B. (1928) *C. botulinum* type D, *Proc. Soc. Exp. Biol. Med. 26*, 88−9.
2. Martin, S. (2003) *Clostridium botulinum* type D intoxication in a dairy herd in Ontario, *Can. Vet. J. 44*, 493−5.
3. Heider, L., McClure, J., and Leger, E. (2001) Presumptive diagnosis of *Clostridium botulinum* type D intoxication in a herd of feedlot cattle, *Can. Vet. J. 42*, 210−2.
4. Coffield, J. A., Bakry, N., Zhang, R., Carlson, J., Gomella, L. G., and Simpson, L. L. (1997) *In vitro* characterization of botulinum toxin types A, C and D action on human tissues: Combined electrophysiologic, pharmacologic and molecular biologic approaches, *J. Pharmacol. Exp. Ther. 280*, 1489−98.
5. Bade, S., Rummel, A., Reisinger, C., Karnath, T., Ahnert-Hilger, G., Bigalke, H., and Binz, T. (2004) Botulinum neurotoxin type D enables cytosolic delivery of enzymatically active cargo proteins to neurons via unfolded translocation intermediates, *J. Neurochem. 91*, 1461−72.
6. Montecucco, C., and Schiavo, G. (1994) Mechanism of action of tetanus and botulinum neurotoxins, *Mol. Microbiol. 13*, 1−8.
7. Schiavo, G., Matteoli, M., and Montecucco, C. (2000) Neurotoxins affecting neuroexocytosis, *Physiol. Rev. 80*, 717−66.
8. Oost, T., Sukonpan, C., Brewer, M., Goodnough, M., Tepp, W., Johnson, E. A., and Rich, D. H. (2003) Design and synthesis of substrate-based inhibitors of botulinum neurotoxin type B metalloprotease, *Biopolymers 71*, 602−19.
9. Schmidt, J. J., Stafford, R. G., and Bostian, K. A. (1998) Type A botulinum neurotoxin proteolytic activity: Development of competitive inhibitors and implications for substrate specificity at the S1′ binding subsite, *FEBS Lett. 435*, 61−4.
10. Schmidt, J. J., and Stafford, R. G. (2005) Botulinum neurotoxin serotype F: Identification of substrate recognition requirements and development of inhibitors with low nanomolar affinity, *Biochemistry 44*, 4067−73.
11. Vaidyanathan, V. V., Yoshino, K., Jahnz, M., Dorries, C., Bade, S., Nauenburg, S., Niemann, H., and Binz, T. (1999) Proteolysis of SNAP-25 isoforms by botulinum neurotoxin types A, C, and E: Domains and amino acid residues controlling the formation of enzyme−substrate complexes and cleavage, *J. Neurochem. 72*, 327−37.
12. Pellizzari, R., Mason, S., Shone, C. C., and Montecucco, C. (1997) The interaction of synaptic vesicle-associated membrane protein/synaptobrevin with botulinum neurotoxins D and F, *FEBS Lett. 409*, 339−42.
13. Santarsiero, B., Yegian, D., Lee, C., Spraggon, G., Gu, J., Scheibe, D., Uber, D., Cornell, E., Nordmeyer, R., Kolbe, W., Jin, J., Jones, A., Jaklevic, J., Schultz, P., and Stevens, R. (2002) An approach to rapid protein crystallization using nanodroplets, *J. Appl. Crystallogr. 35*, 278−81.
14. Otwinowski, Z., and Minor, W. (1997) in *Macromolecular Crystallography*, Part A, pp 307−26, Academic Press: New York.
15. Arndt, J. W., Yu, W., Bi, F., and Stevens, R. C. (2005) Crystal structure of botulinum neurotoxin type G light chain: Serotype divergence in substrate recognition, *Biochemistry 44*, 9574−80.
16. Vagin, A., and Teplyakov, A. (1997) MOLREP: An automated program for molecular replacement, *J. Appl. Crystallogr. 30*, 1022−5.
17. Emsley, P., and Cowtan, K. (2004) Coot: Model-building tools for molecular graphics, *Acta Crystallogr. D60*, 2126−32.
18. Collaborative Computational Project Number 4 (1994) The CCP4 suite: Programs for protein crystallography, *Acta Crystallogr. D50*, 760−3.
19. Brunger, A. T. (1993) Assessment of phase accuracy by cross validation—the free R-value: Methods and applications, *Acta Crystallogr. D49*, 24−36.
20. Breidenbach, M. A., and Brunger, A. T. (2004) Substrate recognition strategy for botulinum neurotoxin serotype A, *Nature 432*, 925−9.
21. Lu, G. G. (2000) TOP: A new method for protein structure comparisons and similarity searches, *J. Appl. Crystallogr. 33*, 176−83.
22. Yamasaki, S., Baumeister, A., Binz, T., Blasi, J., Link, E., Cornille, F., Roques, B., Fykse, E., Sudhof, T., and Jahn, R. (1994) Cleavage of members of the synaptobrevin/VAMP family by types D and F botulinal neurotoxins and tetanus toxin, *J. Biol. Chem. 269*, 12764−72.
23. Monzingo, A. F., and Matthews, B. W. (1984) Binding of N-carboxymethyl dipeptide inhibitors to thermolysin determined

by X-ray crystallography: A novel class of transition-state analogs for zinc peptidases, *Biochemistry 23*, 5724−9.
24. Cai, S. W., and Singh, B. R. (2001) Role of the disulfide cleavage induced molten globule state of type A botulinum neurotoxin in its endopeptidase activity, *Biochemistry 40*, 15327−33.
25. Fu, F. N., Busath, D. D., and Singh, B. R. (2002) Spectroscopic analysis of low pH and lipid-induced structural changes in type A botulinum neurotoxin relevant to membrane channel formation and translocation, *Biophys. Chem. 99*, 17−29.
26. Segelke, B., Knapp, M., Kadkhodayan, S., Balhorn, R., and Rupp, B. (2004) Crystal structure of *Clostridium botulinum* neurotoxin protease in a product-bound state: Evidence for noncanonical zinc protease activity, *Proc. Natl. Acad. Sci. U.S.A. 101*, 6888−93.
27. Hanson, M. A., and Stevens, R. C. (2000) Cocrystal structure of synaptobrevin-II bound to botulinum neurotoxin type B at 2.0 Å resolution, *Nat. Struct. Biol. 7*, 687−92.
28. Agarwal, R., Eswaramoorthy, S., Kumaran, D., Binz, T., and Swaminathan, S. (2004) Structural analysis of botulinum neurotoxin type E catalytic domain and its mutant Glu212 → Gln reveals the pivotal role of the Glu212 carboxylate in the catalytic pathway, *Biochemistry 43*, 6637−44.
29. Agarwal, R., Binz, T., and Swaminathan, S. (2005) Structural analysis of botulinum neurotoxin serotype F light chain: Implications on substrate binding and inhibitor design, *Biochemistry 44*, 11758−65.
30. Rao, K. N., Kumaran, D., Binz, T., and Swaminathan, S. (2005) Structural analysis of the catalytic domain of tetanus neurotoxin, *Toxicon 45*, 929−39.
31. Breidenbach, M. A., and Brunger, A. T. (2005) 2.3 Å crystal structure of tetanus neurotoxin light chain, *Biochemistry 44*, 7450−7.
32. Holm, L., and Sander, C. (1998) Touring protein fold space with Dali/FSSP, *Nucleic Acids Res. 26*, 316−9.
33. Blasi, J., Chapman, E. R., Link, E., Binz, T., Yamasaki, S., Camilli, P. D., Sudhof, T. C., Niemann, H., and Jahn, R. (1993) Botulinum neurotoxin A selectively cleaves the synaptic protein SNAP-25, *Nature 365*, 160−3.
34. Collins, M. D., and East, A. K. (1998) Phylogeny and taxonomy of the food-borne pathogen *Clostridium botulinum* and its neurotoxins, *J. Appl. Microbiol. 84*, 5−17.
35. Hunter, L. C., and Poxton, I. R. (2002) *Clostridium botulinum* types C and D and the closely related *Clostridium novyi*, *Rev. Med. Microbiol. 13*, 75−90.
36. Washbourne, P., Bortoletto, N., Graham, M. E., Wilson, M. C., Burgoyne, R. D., and Montecucco, C. (1999) Botulinum neurotoxin E-insensitive mutants of SNAP-25 fail to bind VAMP but support exocytosis, *J. Neurochem. 73*, 2424−33.
37. Agarwal, R., Binz, T., and Swaminathan, S. (2005) Analysis of active site residues of botulinum neurotoxin E by mutational, functional, and structural studies: Glu335Gln is an apoenzyme, *Biochemistry 44*, 8291−302.
38. Schmidt, J. J., and Bostian, K. A. (1995) Proteolysis of synthetic peptides by type A botulinum neurotoxin, *J. Protein Chem. 14*, 703−8.
39. Breidenbach, M. A., and Brunger, A. T. (2005) New insights into clostridial neurotoxin-SNARE interactions, *Trends Mol. Med. 11*, 377−81.
40. Cornille, F., Deloye, F., Fournié-Zaluski, M.-C., Roques, B. P., and Poulain, B. (1995) Inhibition of neurotransmitter release by synthetic proline-rich peptides shows that the N-terminal domain of vesicle-associated membrane protein/synaptobrevin is critical for neuro-exocytosis, *J. Biol. Chem. 270*, 16826−32.

BI052518R